Title	Numerical Computation of Arc Pressure Distribution(Welding Physics, Process & Instrument)
Author(s)	Fan, Ding; Ushio, Masao; Matsuda, Fukuhisa
Citation	Transactions of JWRI. 15(1) P.1-P.5
Issue Date	1986-07
Text Version	publisher
URL	http://hdl.handle.net/11094/12874
DOI	
rights	本文データはCiNiiから複製したものである
Note	

Numerical Computation of Arc Pressure Distribution†

Ding FAN*, Masao USHIO** and Fukuhisa MATSUDA***

Abstract

Distribution of Gas-Tungsten-Arc pressure distribution is calculated by using the mathematical modelling. The calculated pressure distribution at the anode plate is well consistent with the experimental one.

KEY WORDS: (Arc pressure), (Arc welding), (GTA welding), (Transport phenomena) (Arc simulation), (Plasma flow).

1. Introduction

Arc pressure is one of the most important parameters of arc property in arc welding process. It is not only the influential factor with which the penetration of weld pool is formed, but has a close relationship with fluid flow of arc plasma which governs the stiffness of arc as well.

Some experimental works on arc pressure have already been made[1,2] by measuring the pressure on the anode plate through a small hole, while spatial distribution of arc pressure has not been reported so far, because of the difficulties in the measurement and calculation.

Based on the mathematical model of welding arc which were developed by M. Ushio and MIT group[3,4], the authors have obtained a numerical solutions on spatial distribution of arc pressure by integrating the fluid flow equations in the TIG arc by the use of computer. Through repeating the comparison between computed results and experimentally measured arc pressure at the plate, successive modification of some parameter used in the calculation such as current density profile and electric field distribution, were made and satisfactory agreement has been obtained. Furthermore the effects of electrode shape, arc length and arc current are also calculated and discussed.

Nomenclature

v: Velocity vector
B: Magnetic flux density vector
H: Magnetic field intensity vector
P: Pressure
T: Temperature
S_T: Source term which represents the Joule Heat generation and Radiation loss.
h: Enthalpy
J: Current density vector
F, F_r, F_z: Body force vector and its radial and axial components.
J_r, J_z: Components of current density vector
I: Total arc current
R_0: Arc radius at $z = 0$
R: Arc radius
ρ: Mass density
τ: Stress tensor, which includes both laminar and turbulent stresses.
κ_{eff}: Effective thermal conductivity
μ_{eff}: Effective viscosity
μ_0: Magnetic permiability
δ: Dispersion represents the expansion of current density distribution.

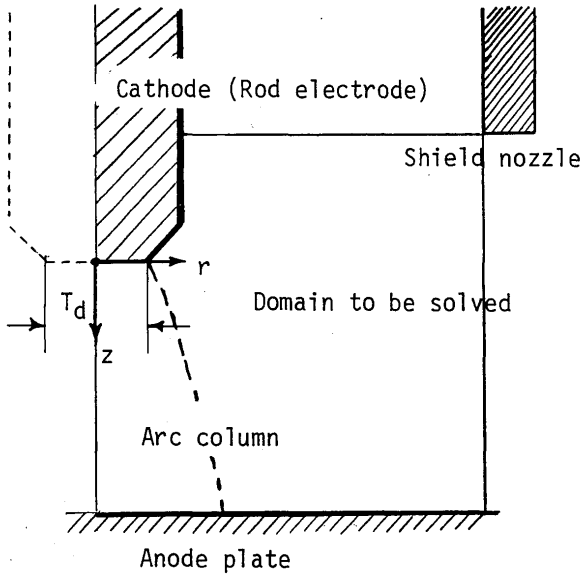

Fig. 1 Schematic drawing of TIG arc model, coordinate system and domain to be solved.

† Received on May 8, 1986.
* Visiting researcher, Gansu University of Technology, China
** Associate Professor
*** Professor

Transactions of JWRI is published by Welding Research Institute of Osaka University, Ibaraki, Osaka 567, Japan

2. Formulation

Figure 1 is a schematic drawing of TIG arc model and coordinate system. A stationary axisymmetric DC arc is applied between a rod electrode and a plate. General governing equations for such a situation take the following form[4].

Equation of continuity:

$$\nabla\cdot(\rho v) = 0 \tag{1}$$

Equation of motion:

$$\rho\,(v\cdot\nabla)\,v = -\nabla p - \nabla\tau + F \tag{2}$$

Thermal energy balance equation:

$$\rho\,(v\cdot\nabla h) = \nabla\cdot\kappa_{eff}\nabla T + S_T \tag{3}$$

Electromagnetic fields and Lorentz force equation:

$$\nabla\cdot H = J \tag{4}$$

$$\nabla\cdot B = 0 \tag{5}$$

$$B = \mu_0 H \tag{6}$$

$$F = J\times B \tag{7}$$

Representing the equation of motion in the axi-symmetric cylindrical coordinate system, we have,

$$\rho\,(v_r\frac{\partial v_r}{\partial r} + v_z\frac{\partial v_r}{\partial z}) = F_r - \frac{\partial P}{\partial r} + [\frac{\partial}{\partial r}\{\frac{\mu_{eff}}{r}\frac{\partial}{\partial r}(rv_r) + \frac{\partial}{\partial z}(\mu_{eff}\frac{\partial v_r}{\partial z})] \tag{8}$$

$$\rho\,(v_r\frac{\partial v_z}{\partial r} + v_z\frac{\partial v_z}{\partial z}) = F_z - \frac{\partial P}{\partial z} + [\frac{1}{r}\frac{\partial}{\partial r}(\mu_{eff}r\frac{\partial v_z}{\partial r}) + \frac{\partial}{\partial z}(\mu_{eff}\frac{\partial v_z}{\partial z})] \tag{9}$$

The pressure difference between any two points can be expressed by

$$P_B - P_A = \int_{A\to B}(\frac{\partial P}{\partial z}dz + \frac{\partial P}{\partial r}dr) \tag{10}$$

Because P concerned here is the isotropical pressure, $P_B - P_A$ must have the same value whatever path is chosen. Sustituting Eqs. (8) and (9) into (10) and making integration we can obtain,

$$P_B - P_A = \int_{A\to B}\{F_z + \frac{1}{r}\frac{\partial}{\partial r}(\mu_{eff}r\frac{\partial v_z}{\partial r}) - \rho v_r\frac{\partial v_z}{\partial r}\}dz + \{(\mu_{eff}\frac{\partial v_z}{\partial z})_B - (\mu_{eff}\frac{\partial v_z}{\partial z})_A\} - \{(\frac{1}{2}\rho v_z^2)_B - (\frac{1}{2}\rho v_z^2)_A\} + \int_{A\to B}\{F_r + \frac{\partial}{\partial z}(\mu_{eff}\frac{\partial v_r}{\partial z}) - \rho v_z\frac{\partial v_r}{\partial z}\}dr + \{[\frac{\mu_{eff}}{r}\frac{\partial}{\partial r}(rv_r)]_B - [\frac{\mu_{eff}}{r}\frac{\partial}{\partial r}(rv_r)]_A\} - \{(\frac{1}{2}pv_r^2)_B - (\frac{1}{2}\rho v_r^2)_A\} \tag{11}$$

3. Solving Procedure

In order to determine the pressure using the Eq. (11), it is necessary to calculate the fluid flow quantities in advance. So the mathematical model described in Ref. (4) was used to obtain the flow field and temperature field of the arc. The current density and arc shape were assumed as follows,

$$J_z = J_0 e\,(-\frac{r^2}{2\delta^2}) \tag{12}$$

$$J_r = -\frac{1}{\mu_0}\frac{\partial B_\theta}{\partial z} \tag{13}$$

$$I = \int_{-\infty}^{\infty} J_z 2\pi r dr \tag{14}$$

$$\delta = R/C_3 \tag{15}$$

$$R = R_0\,[1 + (\frac{z}{R_0})^N] \tag{16}$$

Eq. (16) is the assumed expression for arc shape. The constants C_3, N and R_0 are 0.5, 1.7 and $R_{at\ Z=0} = R_0 = T_d/2$, respectively.

The boundary conditions assumed are the same as those in Ref. (4). The governing equations were put into the dimensionless finite difference forms and integrated over the area defined by the rectangle enclosing a grid point. 41 × 41 non-uniform mesh was used. Introducing the Gauss-Seidel method, point iteration process were carried out until the convergence criterion could be satisfied in all variables.[5]

After then, using the calculated values of fluid flow variables, numerical integrations of Eq. (11) were made along two different paths. The pressure at the upper right corner of the domain to be solved was set to be zero for reference. Then the pressure distribution of the boundary of right side was calculated by using the Eq. (11).

Along the line parallel to r-axis the integration were carried out for all the grid points (P_r). On the otherhand, another integration along the line parallel to z-axis were made from the surface of the electrode ($P = 0$) to the grid points below the electrode and the P_z values were deter-

mined. Finally the averaged value of P_r and P_z was taken as the pressure of the point.

The computation were carried out using the ACOS-900 system of Osaka University.

4. Results and Discussions

A major interest of this paper is to calculate the distribution of arc pressure and through it to make clear the usefulness and weakpoint of the model.

Originally the gas density was assumed to be constant. In the case, it was found that there are comparatively great differences between the calculated arc pressure distribution and experimentally obtained one at the anode plate, and moreover, there is a serious discrepancy between the arc pressure values of a point computed along two different paths of integration.

Later the plasma density was adjusted to be a function of temperature, i.e. $\rho = f(T)$. Under the condition the difference in pressure values computed with different paths of integration is much decreased, particularly in the case of short arc length. And, the pressure distribution calculated agrees well with experimental one at the anode plate.

Figure 2 shows the calculated arc pressure distributions along central axis using two different integration paths. It can be seen the accordance between two curves is comparatively fine, though there is some difference, which may originate from the inappropriateness of integration path for P_z calculation. The P_z was calculated by the integration from the lower surface of electrode, the pressure at which was assumed as zero.

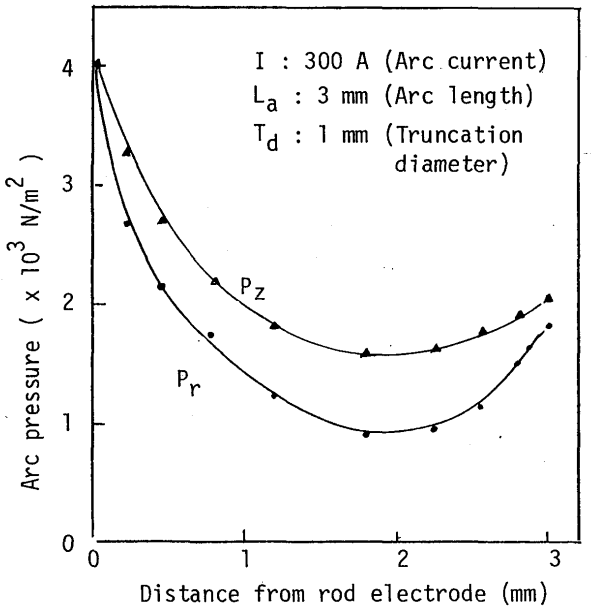

Fig. 2 Pressure distributions along z-axis.
P_r: Integrated along path parallel to r-axis,
P_z: Integrated along path parallel to x-axis.

The radial distribution of arc pressure at the anode plate with different current is shown in **Fig. 3**. It is found that the calculated curve is approximately Gauss-distribution for the current below 250 A, and above the value the curve becomes more sharp owing to much higher current and thus the magnetic force. This agrees very well with experimental result. On the otherhand, the pressure outside of arc is lower than the measured one, which resulted from the sharpness of arc shape. For the comparison, the experimentally obtained arc pressure are shown in **Figures 4** and **5**.

Figure 6 shows the arc pressure distribution along z-axis with different current. The pressure has a maximum just below the electrode tip, and a minimum in the arc column in front of the plate. In other words, there is a sharp decrease in arc pressure near the rod electrode and it begins to increase at around the point of 1 mm from the plate. This behavior is very similar for the arcs with four different currents except the change in the magnitude.

The arc pressure consists of the magnetic force term, viscous force term and inertial force term as shown in Eq. (2). In the zone near rod electrode, the current density, thereby the magnetic force is very high. This high force-field induces and accelerates the flow of plasma gas. With increase in velocity of fluid, the dynamic pressure and viscous consumption increase, and therefore the isotropic pressure decreases. While in the zone near the plate the fluid flow velocity decreases and stagnates due

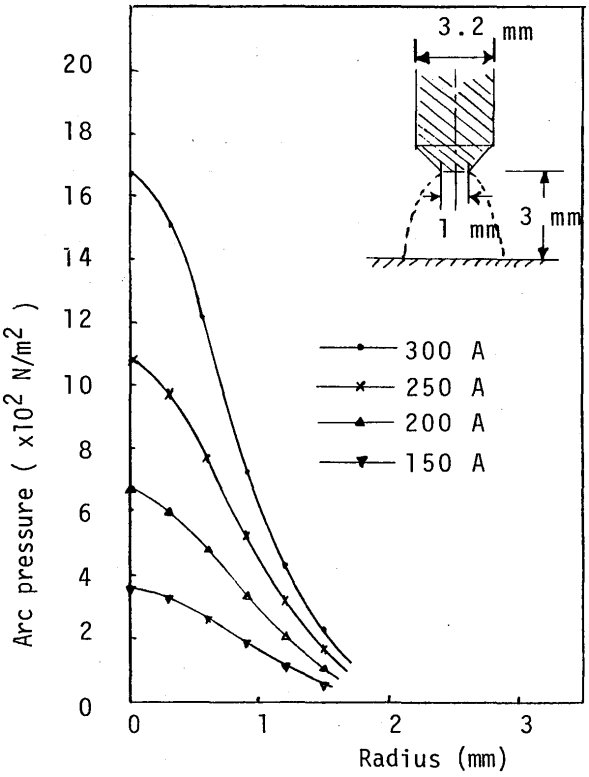

Fig. 3 Arc pressure distribution on the anode plate for different arc current.

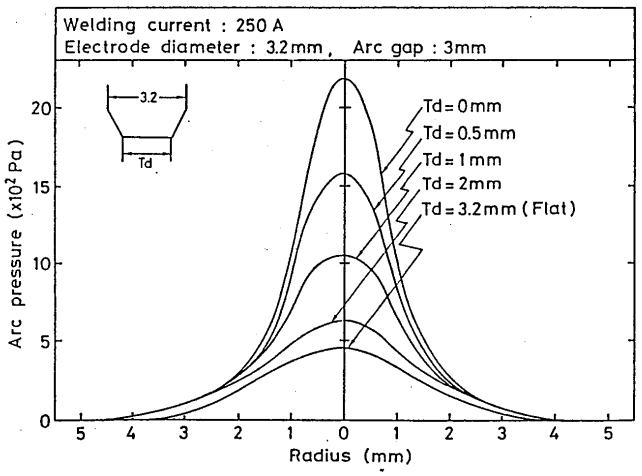

Fig. 4 Experimentally obtained arc pressure distribution at the anode plate.

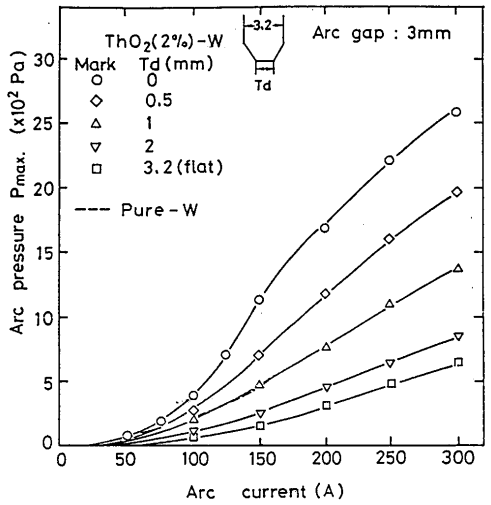

Fig. 5 Experimentally measured maximum arc pressure at th anode and its dependence on the arc current and truncation diameter of the electrode.

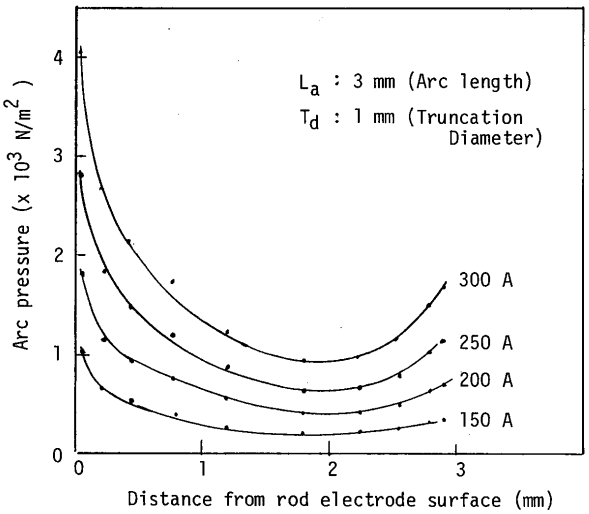

Fig. 6 Calculated arc pressure distribution along z-axis for various arc currents.

to the obstruction of plate, thus the isotropic pressure increases.

The influences of arc length on pressure distribution are presented in **Figs. 7** and **8**. It can be seen that the long arc presents a lower and blunt arc pressure distribution in the area near plate. This behavior was confirmed by experimental measurement of the arc pressure. It can be attributable to the higher development of flow field, great viscous consumption and the expansion in arc column cross section near the plate.

Some attempts has also been made on the calculation of the influence of electrode shape on pressure distribution. The results show the pressure increase when the shape is changed from a flat one to a truncated cone, and a pointed one. This is consistent with experimental results but the quantitative agreement between calculated one and experimental results was not satisfactory. It may be

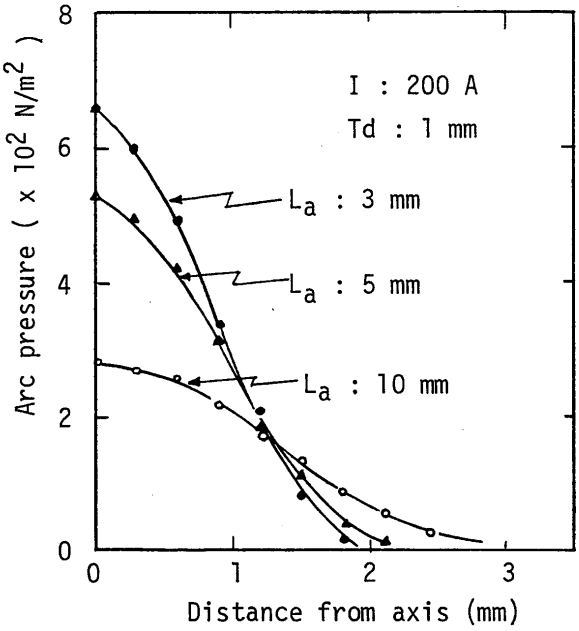

Fig. 7 Calculated arc pressure distribution on the anode plate, that shows the effect of arc current.

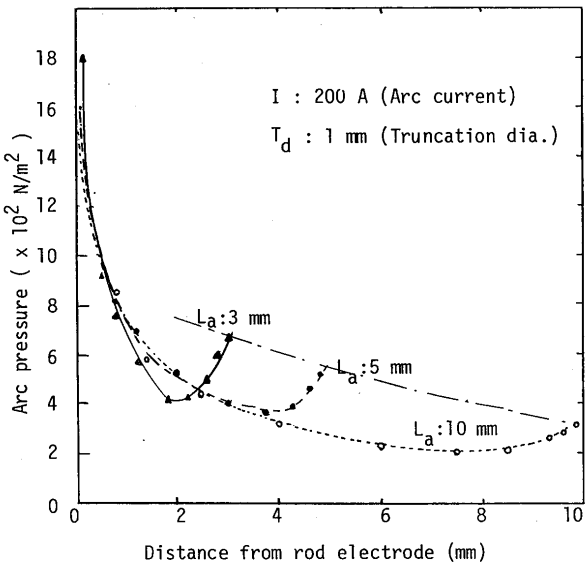

Fig. 8 Effect of arc length on arc pressure distribution along z-axis.

resulted from the oversimplification of arc current density distribution, arc shape and some physical constants.

5. Conclusions

1) The arc pressure in GTA welding was calculated by using the mathematical model of arc. The calculated arc pressure distribution at anode plate is well consistent with experimental results.
2) The arc pressure distributions along z-axis has a maximum value just below the electrode tip and a minimum value in the arc column at the point about 1 mm apart from plate.
3) The long arc has a lower pressure distribution though the effect is very small in the zone near the rod electrode.

References

1. Yamauchi, N. and Taka, T., IIW Doc. 212-452-79, (1979).
2. Selyanenkov, V.N. et al., Svar. Proiz No. 5 (1980), pp-5.
3. Chang, C.W., Eager, T.W. and Szekely, J., Proc. Int. Conf. Arc Physics and Weld pool behavior, Paper No. 13 (1979), TWI, London.
4. Ushio, M. and Matsuda, F., Trans. JWRI, Vol. 11, No. 1 (1982) pp-7.
5. Gosman, A.D. et al., "Heat and Mass Transfer in Recirculating Flows", Academic Press (1969).